

Super-Gaussian, superdiffusive transport of multimode active matterSeungsoo Hahn ^{1,2}, Sanggeun Song ^{2,3,4}, Gil-Suk Yang,^{2,4} Jingyu Kang,^{2,3,4} Kang Taek Lee,^{5,*} and Jaeyoung Sung ^{2,3,4,†}¹*Da Vinci College of General Education, Chung-Ang University, Seoul 06974, Korea*²*Creative Research Initiative Center for Chemical Dynamics in Living Cells, Chung-Ang University, Seoul 06974, Korea*³*Department of Chemistry, Chung-Ang University, Seoul 06974, Korea*⁴*National Institute of Innovative Functional Imaging, Chung-Ang University, Seoul 06974, Korea*⁵*Department of Chemistry, Gwangju Institute of Science and Technology, Gwangju 61005, Korea*

(Received 19 March 2020; revised 7 August 2020; accepted 2 September 2020; published 19 October 2020)

Living matter often exhibits multimode transport that switches between an active, self-propelled motion and a seemingly passive, random motion. Here, we investigate an exactly solvable model of multimode active matter, such as living cells and motor proteins, which alternately undergoes active and passive motion. Our model study shows that the reversible transition between a passive mode and an active mode causes super-Gaussian transport dynamics, observed in various experiments. We find the non-Gaussian character of the matter's displacement distribution is essentially determined by the population ratio between active and passive motion. Interestingly, under a certain population ratio of the active and passive modes, the displacement distribution changes from sub-Gaussian to super-Gaussian as time increases. The mean-square displacement of our model exhibits transient superdiffusive dynamics, yet recovers diffusive behavior at both the short- and long-time limits. We finally generalize our model to encompass complex, multimode active matter in an arbitrary spatial dimension.

DOI: [10.1103/PhysRevE.102.042612](https://doi.org/10.1103/PhysRevE.102.042612)**I. INTRODUCTION**

Active matter, such as motor proteins, living cells, and Janus nanoparticles, consumes energy for its motion; in many cases, active matter exhibits multiple transport modes: a seemingly passive mode showing undirected, random motion and active modes for self-propelled, systematic motion [1–4]. The regulatory state of active matter or the heterogeneous environment surrounding active matter causes a stochastic transition between biological modes, which has been widely observed in various biological processes [3–9]. However, there also exists active matter with only an active mode. This type of active matter often shows a run-and-reverse motion, in which the active matter moves in one direction for a period of time and moves in the opposite direction for the next period [10,11]. Active matter motion with multiple modes or a run-and-reverse type of motion has been observed for various systems including cargo and vesicles in living cells and bacterial cell systems [10–16].

Active matter generally exhibits anomalous, non-Gaussian transport dynamics, which is in contrast to passive thermal motion described by Einstein's theory of Brownian motion [2,17,18]. However, various models based on this theory have been used to explain the long-time behavior of the mean-square displacement (MSD) of active matter observed in experiments, where the MSD is linearly proportional to measurement time [19,20]. Although these models assume

that active matter motion is qualitatively the same as passive thermal motion, in many cases, they provide a satisfactory explanation of experimental results for the MSD at long times. However, the short-time dynamics of active matter measured by the MSD and the non-Gaussian displacement distribution cannot be explained by those models based on the conventional theory of Brownian motion [21,22].

Various experimental studies have shown that active matter motion is superdiffusive, that is, the MSD of active matter is proportional to t^α with $\alpha > 1$ [1,4,14,15]. To delineate this superdiffusive behavior of active matter, mathematical models involving Levy walks have been proposed [23–27]. Alternative models to account for the superdiffusive transport dynamics of active matter are the active Brownian particle model [28,29] and the run-and-reverse motion model [30]. These models do provide an enhanced explanation for the anomalous MSD of active particles; however, the above-mentioned models cannot explain the super-Gaussian displacement distribution of active matter, whose kurtosis is greater than that of a Gaussian [2,31].

In this work, we introduce an exactly solvable model of active matter which can exhibit a super-Gaussian displacement distribution. This behavior of our active matter model is consistent with the previous observations that active matter shows diffusive dynamics both at short times and at long times but with a greater diffusion coefficient at long times [2,5,19,20] and transient superdiffusion at the intermediate times [32–34]. The key feature of our active matter model is that it undergoes self-propelled motion and diffusive motion alternatively. Similar models have been investigated in the context of intermittent search strategies [35–39], reaction

*ktlee@gist.ac.kr

†jaeyoung@cau.ac.kr

kinetics [7], transport of membrane protein [40,41], and diffusion in randomly switching environments [42–44]. However, to the best of our knowledge, there has not yet been rigorous study on the non-Gaussian character of the displacement distribution of multimode active matter.

From our exactly solvable model study, we find that the population ratio of the passive diffusive mode to the active, self-propelled mode determines the type of displacement distribution to be sub-Gaussian (kurtosis < 3) or super-Gaussian (kurtosis > 3). In a certain range of the population ratio, the displacement distribution can change from sub-Gaussian to super-Gaussian over time. We also present a generalization of this one-dimensional model into higher spatial dimensions.

II. THEORETICAL MODELS

We first consider a simple one-dimensional model of multimode active matter, which is relevant to the motor proteins moving along the microtubule [2]. In the high-friction regime, where we can neglect the inertial term in the Langevin equation, the velocity, $\dot{x}(t)$, of our multimode active matter model is written as the sum of two components:

$$\dot{x}(t) = v_{s,\Gamma}(t) + v_{\xi}(t), \quad (1)$$

where $v_{s,\Gamma}(t)$ and $v_{\xi}(t) [\equiv \gamma^{-1} \xi(t)]$ represent the velocity component of self-propelled, ballistic motion, whose value depends on internal state Γ of active matter, and the velocity component caused by the random fluctuating force, $\xi(t)$. γ denotes the friction constant. As usual, we model the dynamics of $\xi(t)$ as Gaussian white noise, whose time correlation, $\langle \xi(t+t_0)\xi(t_0) \rangle$, is linearly proportional to the Dirac delta function. On the other hand, the dynamics of $v_s(t)$ is coupled to transitions between states of the multimode active matter so that the relaxation of $\langle v_s(t+t_0)v_s(t_0) \rangle$ from the initial value, $\langle v_s^2 \rangle$, to the final value, $\langle v_s \rangle^2$, occurs in the timescale of the state dynamics of our active matter, which is far longer than the fluctuation timescale of the random force $\xi(t)$. This theoretical model captures the essential features observed in the transport dynamics of experimentally observed motion of the motor protein complex on the microtubule [2]. Later in this work, we extend this model to describe multimode active matter moving in higher spatial dimensions.

In our model, we assume that there exist internal state variables, Γ , that are often beyond our ability to observe but coupled to the self-propelled velocity and hence the displacement of active matter. We model the dynamics of the hidden state variables as a multidimensional Markov process. Then, the Fokker-Planck equation corresponding to Eq. (1) is given by

$$\begin{aligned} \frac{\partial}{\partial t} P(\Gamma, x, t) &= \frac{\partial}{\partial x} \left[D_0 \frac{\partial}{\partial x} - v_s(\Gamma) \right] P(\Gamma, x, t) \\ &+ L(\Gamma) P(\Gamma, x, t), \end{aligned} \quad (2)$$

where $P(\Gamma, x, t)$ denotes the probability density function (PDF) of active matter at position x , at hidden state Γ , and at time t [45–48]. In Eq. (2), D_0 stands for the diffusion coefficient of passive motion originating from the random fluctuating force defined by $D_0 = \int_0^\infty dt \langle v_{\xi}(t)v_{\xi}(0) \rangle$ [49].

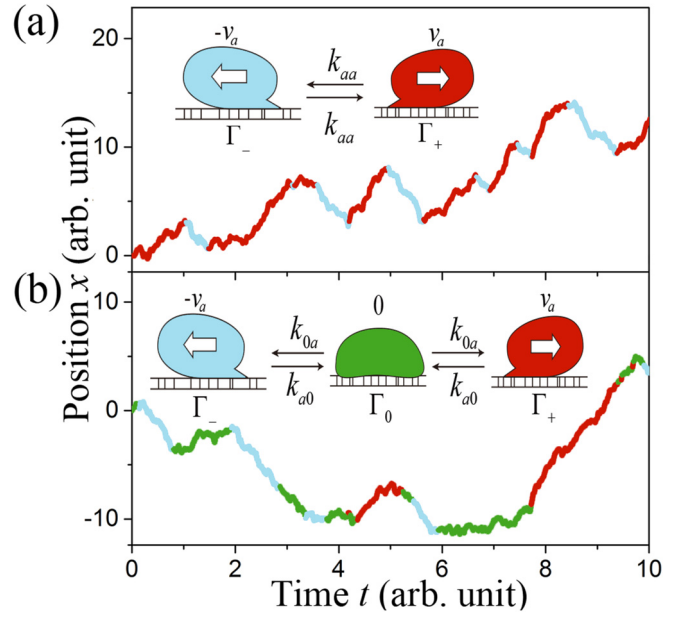


FIG. 1. Model systems and typical trajectories. (a) The single-mode model consists of two internal states, Γ_+ and Γ_- . The single-mode active matter in state Γ_{\pm} performs self-propelled, directed motion with velocity $\pm v_a$ despite a random force exerted from the medium. Stochastic transitions between the internal states occur with a constant rate, k_{aa} . (b) The multimode model consisting of three internal states: passive motion state, Γ_0 , in addition to active motion states, Γ_+ and Γ_- . The multimode active matter performs undirected, random motion in state Γ_0 , but performs directed, self-propelled motion with velocity $\pm v_a$ in state Γ_{\pm} . k_{0a} and k_{a0} represent the stochastic transition rates from the passive Γ_0 to the active Γ_{\pm} state and from the active Γ_{\pm} to the passive Γ_0 state, respectively. For each model, a typical time trace of active matter position is delineated. Colors in the active matter diagram and trajectory represent the cell's internal states.

$L(\Gamma)$ in Eq. (2) denotes a mathematical operator describing hidden state dynamics [47,48].

We now compare two simple, exactly solvable models of active matter (Fig. 1): one for single-mode active matter, which undergoes both diffusion and run-and-reverse motion [13,30,50,51] at the same time, and another for multimode active matter that undergoes pure diffusion and self-propelled motion in an alternating manner. Our multimode active matter model is relevant to intermittent search strategies [35,37] and the multimode motor protein multiplex model [2].

For our single-mode model shown in Fig. 1(a), active matter has two hidden states, Γ_+ and Γ_- , at which active matter undergoes active motion in the positive and negative directions, respectively. For the sake of simplicity, the transitions between the two hidden states are assumed to be Poisson processes. For this model, Eq. (2) becomes

$$\begin{aligned} \frac{\partial}{\partial t} \begin{pmatrix} P_+(x, t) \\ P_-(x, t) \end{pmatrix} &= \frac{\partial}{\partial x} \left[\frac{\partial}{\partial x} D_0 \mathbf{I} - \begin{pmatrix} v_a & 0 \\ 0 & -v_a \end{pmatrix} \right] \begin{pmatrix} P_+(x, t) \\ P_-(x, t) \end{pmatrix} \\ &+ \begin{pmatrix} -k_{aa} & k_{aa} \\ k_{aa} & -k_{aa} \end{pmatrix} \begin{pmatrix} P_+(x, t) \\ P_-(x, t) \end{pmatrix}, \end{aligned} \quad (3)$$

where $P_{\pm}(x, t)$ denotes the probability density that active matter is at position x , at hidden state Γ_{\pm} , and at time t [see Appendix A for the derivation of Eq. (3)]. In Eq. (3), $\pm v_a$ and k_{aa} denote the velocity, $v_s(\Gamma_{\pm})$, of the self-propelled motion of the active matter at state Γ_{\pm} and the transition rate between the two hidden states, Γ_+ and Γ_- .

On the other hand, the multimode model shown in Fig. 1(b) has three hidden states, Γ_+ , Γ_- , and Γ_0 at which active matter undergoes self-propelled active motion in the positive and negative directions, and passive random motion, respectively. For this model, Eq. (2) reads as

$$\frac{\partial}{\partial t} \begin{pmatrix} P_+(x, t) \\ P_0(x, t) \\ P_-(x, t) \end{pmatrix} = \frac{\partial}{\partial x} \left[\frac{\partial}{\partial x} D_0 \mathbf{I} - \begin{pmatrix} v_a & 0 & 0 \\ 0 & 0 & 0 \\ 0 & 0 & -v_a \end{pmatrix} \right] \begin{pmatrix} P_+(x, t) \\ P_0(x, t) \\ P_-(x, t) \end{pmatrix} + \begin{pmatrix} -k_{a0} & k_{0a} & 0 \\ k_{a0} & -2k_{0a} & k_{a0} \\ 0 & k_{0a} & -k_{a0} \end{pmatrix} \begin{pmatrix} P_+(x, t) \\ P_0(x, t) \\ P_-(x, t) \end{pmatrix}. \quad (4)$$

In Eq. (4), $P_i(x, t)$ designates the probability density of matter at hidden state Γ_i ($i \in +, -, 0$) and at position x at time t . $\pm v_a$ has the same meaning as in Eq. (3). k_{0a} and k_{a0} denote, respectively, the transition rate from state Γ_0 , at which $v_s(\Gamma_0) = 0$, to either state, Γ_+ or Γ_- , and the transition rate from state Γ_{\pm} to state Γ_0 , respectively. Typical time traces are depicted for the two models in Fig. 1. Exact analytic solutions of Eqs. (3) and (4) can be obtained in the Fourier domain as given in Eqs. (C3) and (B4) in Appendix C and B, respectively.

III. MEAN VELOCITY DISTRIBUTION

From the exact solutions, we obtain the distribution, $f(\bar{v}, t)$, of the mean velocity, defined by $x(t)/t (\equiv \bar{v}(t))$. The mean velocity distribution is related to the displacement distribution $P(x, t)$ by $P(x, t) = t^{-1} f(x/t, t)$. The shape of $f(\bar{v}, t)$ changes over time. The characteristic relaxation time, τ_c , defined by $\tau_c \equiv \int_0^{\infty} dt \phi_{v_s}(t)$ with $\phi_{v_s}(t) \equiv \langle v_s(t)v_s(0) \rangle / \langle v_s^2 \rangle$, is a criterion for determining the shape of the distributions. The analytic expression of τ_c is dependent on the model in question. For the single-mode model, τ_c is given by half the lifetime of active states Γ_{\pm} , i.e., $\tau_c = (2k_{aa})^{-1}$. For the multimode model, τ_c is the same as the lifetime, k_{a0}^{-1} , of the state Γ_{\pm} (see Appendices D and E). The PDFs of the displacements at short and long times are derived in Appendix F.

At times much shorter than τ_c , the mean velocity distribution can be approximated by a linear combination of Gaussians centered at the state-dependent self-propelled velocity, $v_s(\Gamma_i)$, for both models (see Appendices G and H), that is

$$f(\bar{v}, t) \cong \sum_i p_i^{eq} (4\pi D_0 t)^{-1/2} \times \exp[-(\bar{v} - v_s(\Gamma_i))^2 / (4D_0 t)] \quad (t \ll \tau_c), \quad (5)$$

where p_i^{eq} denotes the equilibrium probability of state Γ_i , given by $p_{\pm}^{eq} = 1/2$ for the single-mode model and by $p_{\pm}^{eq} = k_{0a}/(k_{a0} + 2k_{0a})$ and $p_0^{eq} = k_{a0}/(k_{a0} + 2k_{0a})$ for the multimode model. Equation (5) can also be obtained from the distribution of the instantaneous velocity given in Eq. (1), because the mean velocity, $x(t)/t$, is the same as the instantaneous

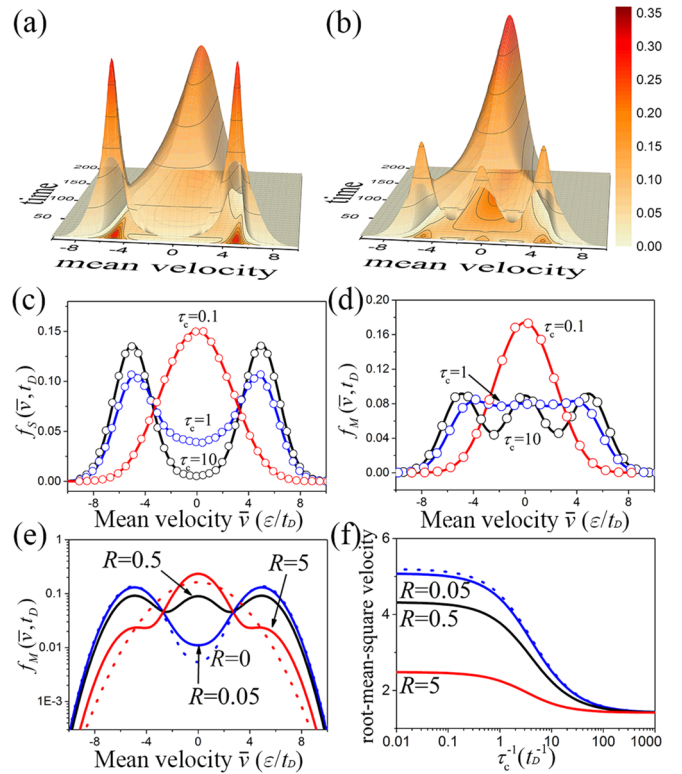


FIG. 2. PDFs for mean velocity distribution. The time-dependent mean velocity distribution, (a) $f_S(\bar{v}, t)$ for the single-mode model and (b) $f_M(\bar{v}, t)$ for the multimode model with the population ratio of the passive state to the active states being $R = 0.5$. In both (a) and (b), the mean velocity distribution is displayed starting from time $t = t_D (\equiv \varepsilon^2/D_0)$; the relaxation time τ_c of the velocity-velocity autocorrelation function is set to be $10t_D$. ε denotes a length unit. The unit of time is t_D . (c), (d) The mean velocity distribution at $t = t_D$ (c) for the single-mode model and (d) for the multimode model, with three different values of τ_c (in t_D unit); (lines) analytic results, and (circles) stochastic simulation results (see Appendix K). In (d), the value of R is set to be 0.5, for which the three states of the multimode model are equally probable at equilibrium, i.e., $p_{\pm}^{eq} = p_0^{eq} = 1/3$. (e) The mean velocity distributions at $t = t_D$ for the multimode model with four different values of R : (blue dotted line) $R = 0$; (blue solid line) $R = 0.05$; (black line) $R = 0.5$; and (red line) $R = 5$. The Gaussian distribution with the same mean and variance as $f_M(\bar{v}, t_D)$ for $R = 5$ is plotted as a red dotted line. The value of τ_c is set to be $10t_D$. (f) Dependence of the root-mean-square velocities, or the standard deviation of the mean velocity distributions on the relaxation rate, τ_c^{-1} , are displayed for four different values of R represented in (e). In our length and time units, the value of D_0 is unity. The values of the other parameter is set to be $v_a = 5 \varepsilon/t_D$ for all cases.

velocity in the short-time limit (see Appendix H). As shown in Figs. 2(a) and 2(b), the mean velocity distribution, $f_S(\bar{v}, t)$, of the single-mode model has two Gaussian peaks centered at $\pm v_a$ and $-v_a$ at short times ($t \ll \tau_c$). In comparison, the mean velocity distribution, $f_M(\bar{v}, t)$, of the multimode model has an additional Gaussian peak centered at 0, resulting from the state Γ_0 . The variance of each Gaussian peak is approximately given by $2D_0/t$.

At times much longer than the characteristic time τ_c , the mean velocity distribution becomes a single-peaked Gaussian distribution centered at the initial position for both the single-mode and multimode models of active matter. As shown in Figs. 2(a) and 2(b), both $f_S(\bar{v}, t)$ and $f_M(\bar{v}, t)$ converge to a Gaussian distribution with a variance proportional to $t^{-1/2}$ at long times. That is to say, for both models, the distribution of $x(t)/\sqrt{t}$ approaches Gaussian at long times, in accordance with the Gaussian central limit theorem (see Appendix G). Taking a different approach, the mean velocity distribution converges more quickly to the long-time asymptotic Gaussian distribution as the value of τ_c decreases [see Figs. 2(c) and 2(d)]. In the small- τ_c limit, the mean velocity distribution is Gaussian at any finite time.

The mean velocity distribution, $f_M(\bar{v}, t)$, of the multimode model is also dependent on the lifetime, $\tau_0 (\equiv 1/(2k_{0a}))$, of passive state Γ_0 , as well as on the lifetime, $\tau_a (\equiv 1/k_{a0} = \tau_c)$, of active states Γ_{\pm} . As shown in Fig. 2(e), when the population ratio, $R (\equiv p_0^{eq}/(p_+^{eq} + p_-^{eq}) = \tau_0/\tau_a = k_{a0}/(2k_{0a}))$, of passive state to active states decreases, $f_M(\bar{v}, t)$ approaches $f_S(\bar{v}, t)$ (see Appendix I). However, as the value of R increases, the peak centered at $\bar{v} = 0$ in $f_M(\bar{v}, t)$ grows large, so that the MSD of the multimode model is smaller than the MSD of the single-mode model.

Note also that the variance of the mean velocity, $\langle \delta \bar{v}^2 \rangle (\equiv \langle \delta x^2 \rangle / t^2)$, decreases with the relaxation rate, τ_c^{-1} , of the fluctuation in the self-propelled velocity, as shown in Fig. 2(f). This is a common feature of dynamically disordered systems and is called motional narrowing in spectroscopy [52].

IV. MEAN-SQUARE DISPLACEMENT AND NON-GAUSSIAN PARAMETER

For both the models, the mean-square displacement shows three different kinetic phases: short-time diffusion, intermediate transient superdiffusion, and long-time diffusion with a greater diffusion coefficient, in agreement with previously reported experimental results [32,33]. Exact analytic expressions of the MSD, $\langle x^2(t) \rangle$, for both models can be decomposed into two diffusion components, namely the MSD from the random fluctuating force ($\langle x_{\xi}^2(t) \rangle$) and the MSD from self-propelled motion ($\langle x_{v_s}^2(t) \rangle$). The resulting MSD is then written as

$$\begin{aligned} \langle x^2(t) \rangle &= \langle x_{\xi}^2(t) \rangle + \langle x_{v_s}^2(t) \rangle \\ &= 2D_0t + 2D_a\tau_c(e^{-t/\tau_c} - 1 + t/\tau_c), \end{aligned} \quad (6)$$

where D_a is the additional diffusion coefficient component contributed from self-propelled motion, defined by $D_a \equiv \int_0^{\infty} dt \langle v_s(t)v_s(0) \rangle = \tau_c v_a^2 p_a$. Here, p_a designates the probability of active states, which is unity for the single-mode model and $p_a = p_+^{eq} + p_-^{eq} = (1+R)^{-1}$ for the multimode model. D_0 and τ_c have the same meaning as in the previous section. See Appendices B and E for two different derivations of Eq. (6). As shown in Fig. 3(a), the MSD is given by $\langle x^2(t) \rangle \cong 2D_0t = \langle x_{\xi}^2(t) \rangle$ at short times ($t \ll \tau_c$) and is dominantly contributed from passive, random motion. On the other hand, at long times ($t \gg \tau_c$), the MSD is given by $\langle x^2(t) \rangle \cong 2(D_0 + D_a)t$, with the diffusion coefficient in-

creased by D_a . At intermediate times ($t \approx \tau_c$), the MSD of our model shows a transient superdiffusive behavior where the value of $\alpha(t) [\equiv d \ln \langle x^2(t) \rangle / d \ln t]$ is significantly greater than unity. For our model, the value of $\alpha(t)$ is actually greater than unity at all times; however, at both the short-time limit and the long-time limit, the value of $\alpha(t)$ approaches unity and the apparent dynamics of our model follows Fickian diffusion.

In the early stage of the intermediate regime, the MSD is approximately a quadratic function of time ($\alpha = 2$), i.e., $\langle x^2(t) \rangle \cong 2D_0t + D_a\tau_c(t/\tau_c)^2$, shown by the green lines in Fig. 3(b), which originates from ballistic, self-propelled motion of active matter. This ballistic motion diminishes as the velocity autocorrelation function, e^{-t/τ_c} , decreases, and the dynamics of the multimode active matter changes from superdiffusive motion to normal diffusive motion. As shown in Eq. (6), the mean-square displacement resumes diffusive behavior faster as the characteristic relaxation time τ_c of the velocity autocorrelation function decreases.

An equation similar to Eq. (6) has been reported in many other studies because the equation can be derived based on two simple assumptions: first, overall movement is composed of two independent movements with different relaxation timescales; second, the velocity autocorrelation can be represented by an exponential function [53–56]. Because our models also include these assumptions, both models yield the same analytic results for MSDs, but the two models can have far different displacement distributions.

The displacement distribution, $P_M(x, t)$, of the multimode model can be super-Gaussian, which is in accordance with the experimental data reported in Refs. [2,31], whereas $P_S(x, t)$ of the single-mode model is always sub-Gaussian. For the multimode model, the non-Gaussian parameter (NGP), a measure of the deviation of the displacement distribution from Gaussian, is sensitive to the population ratio, R , of the passive state to the active states, which is shown in Fig. 3(c). The exact analytic expression of the time-dependent NGP, defined as $[\langle x^4(t) \rangle / 3 \langle x^2(t) \rangle^2] - 1$, is given in Eq. (B8) of Appendix B. The short-time and long-time asymptotic expressions of NGP are given by

$$\text{NGP}_R(t) \cong \begin{cases} \frac{1}{12} \frac{(R-2)}{(R+1)^2} \left(\frac{D_a^{(0)}}{D_0} \right)^2 (t/\tau_c)^2, & t \ll \tau_c, \\ 2 \frac{R^2 - R - 1}{(R+1)^3} \left(\frac{D_a^{(0)}}{D_0 + D_a} \right)^2 \frac{\tau_c}{t}, & t \gg \tau_c, \end{cases} \quad (7)$$

where $D_a^{(0)}$ designates $\tau_c v_a^2$, or the value of D_a in the limit where active matter is always in active states. According to Eq. (7), the displacement distribution, $P_M(x, t)$, of multimode active matter is super-Gaussian when $R > 2$, but sub-Gaussian when $R < (1 + \sqrt{5})/2 \cong 1.62$ at all times, which is found to be the case for the multimode model as shown in Fig. 3(d). When $(1 + \sqrt{5})/2 \cong 1.62 < R < 2$, the displacement distribution of the multimode model shows an interesting switching behavior from the short-time sub-Gaussian distribution to super-Gaussian distribution, as shown in Fig. 4(a). In this special case, the displacement distribution is sub-Gaussian at times shorter than τ_c but super-Gaussian at times longer than τ_c as demonstrated in Fig. 4(b).

Note that $\text{NGP}_R(t)$ vanishes in the large- R limit, in which the multimode matter is always in the passive state. This means that, in our model, it is self-propelled,

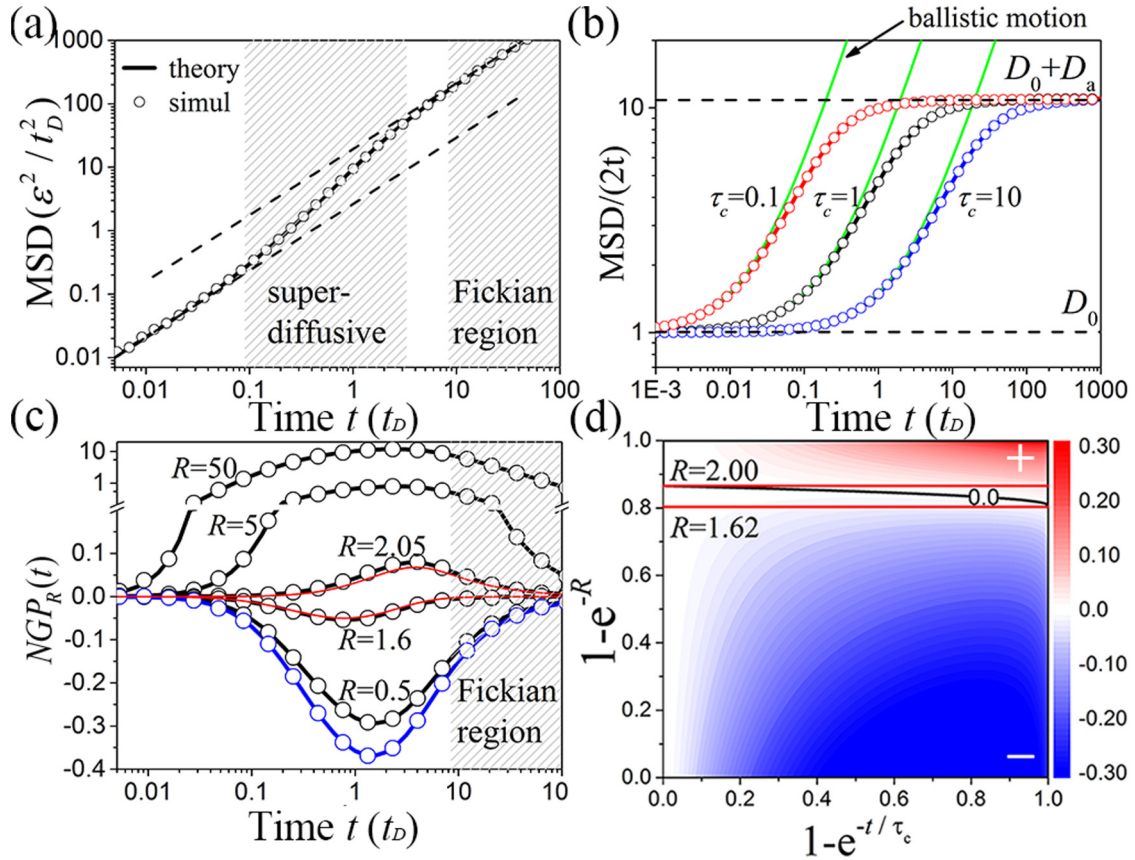


FIG. 3. Mean-square displacement and non-Gaussian parameter. (a) Time-dependent MSD: (lines) analytic results, (circles) stochastic simulation results. The single-mode and multimode models share the same MSD, given in Eq. (6). In the model calculation, the value of τ_c is set equal to t_D . As in Fig. 2, the value of D_0 is unity. The value of $D_a (= \tau_c v_a^2 p_a)$ is set to be $10 D_0$. For both single-mode and multimode models, the MSD exhibits the same superlinear time dependence; the value of $\alpha(t) [\equiv d \ln \langle x^2(t) \rangle / d \ln t]$ is greater than unity at all times. However, at both short-time and long-time limits, the value of $\alpha(t)$ approaches unity. (b) Time dependence of $\langle x^2(t) \rangle / 2t$ for the three different values of τ_c : (red line) $\tau_c = 0.1 t_D$, (black line) $\tau_c = t_D$, and (blue line) $\tau_c = 10 t_D$. The effective diffusion coefficient increases from D_0 to $D_0 + D_a$, whose transition timescale is determined by τ_c . The green line represents the ballistic motion ($\langle x^2(t) \rangle \cong 2D_0 t + D_a \tau_c (t/\tau_c)^2$) for each case. (c) Time dependence of the non-Gaussian parameter for the single-mode model (blue line) and for the multimode models with various values of R (black lines), where the time profile of the MSD is kept the same as shown in (a). The two red lines represent the non-Gaussian parameter, $\text{NGP}_R(t)$, for the two critical values of R , 1.62 and 2. When $R < 1.62$ ($R > 2.00$) the displacement distribution is sub-Gaussian (super-Gaussian) at all times. (d) $\text{NGP}_R(t)$ for the entire range of R and time. The value of $\lim_{R \rightarrow 0} D_a = D_a^{(0)} (\equiv \tau_c v_a^2)$ is set to be $10 D_0$. The two horizontal red lines represent $\text{NGP}_R(t)$ for the two limit values of R . When the value of R is between 1.62 and 2, the displacement distribution switches from sub-Gaussian to super-Gaussian as the time increases. The boundary between the sub-Gaussian regime and the super-Gaussian distribution regime is represented by the black line.

ballistic motion that causes the displacement distribution to be non-Gaussian. In the opposite, small- R limit, $P_M(x, t)$ has exactly the same shape as $P_S(x, t)$ as shown in Appendix I; consequently, $\text{NGP}_R(t)$ of the multimode model reduces to $\text{NGP}_0(t) [\equiv \lim_{R \rightarrow 0} \text{NGP}_R(t)]$ of the single-mode model, whose asymptotic behavior is given by

$$\text{NGP}_0(t) \cong \begin{cases} -\frac{1}{6} \left(\frac{D_a^{(0)}}{D_0} \right)^2 (t/\tau_c)^2, & t \ll \tau_c. \\ -2 \left(\frac{D_a^{(0)}}{D_0 + D_a^{(0)}} \right)^2 \frac{\tau_c}{t}, & t \gg \tau_c. \end{cases} \quad (8)$$

Equation (8) clearly shows that the displacement distribution, $P_S(x, t)$, of single-mode active matter is always sub-Gaussian. This sub-Gaussian displacement distribution for single-mode active matter has been reported in other studies, which show that perpetual self-propelled motion with

orientational relaxation in two-dimensional space generates a sub-Gaussian displacement distribution [53,56,57].

In general, the NGP of the multimode active matter whose motion obeys the Langevin equation, Eq. (1), can be written as

$$\text{NGP}_R(t) = \frac{\langle x_{v_s}^2(t) \rangle^2}{\langle x^2(t) \rangle^2} \text{NGP}_{R, v_s}(t), \quad (9)$$

where $\text{NGP}_{R, v_s}(t) [\equiv \langle x_{v_s}^4(t) \rangle / (3 \langle x_{v_s}^2(t) \rangle^2) - 1]$ denotes the NGP originating from self-propelled active motion. At short times, $\text{NGP}_{R, v_s}(t)$ can be approximated by a constant value, $(R-2)/3$, while the ratio, $\langle x_{v_s}^2(t) \rangle^2 / \langle x^2(t) \rangle^2 [\equiv (D_a^{(0)} t / 2D_0 \tau_c (R+1))^2]$, is proportional to t^2 . This result explains the quadratic time dependence of $\text{NGP}_R(t)$ at short

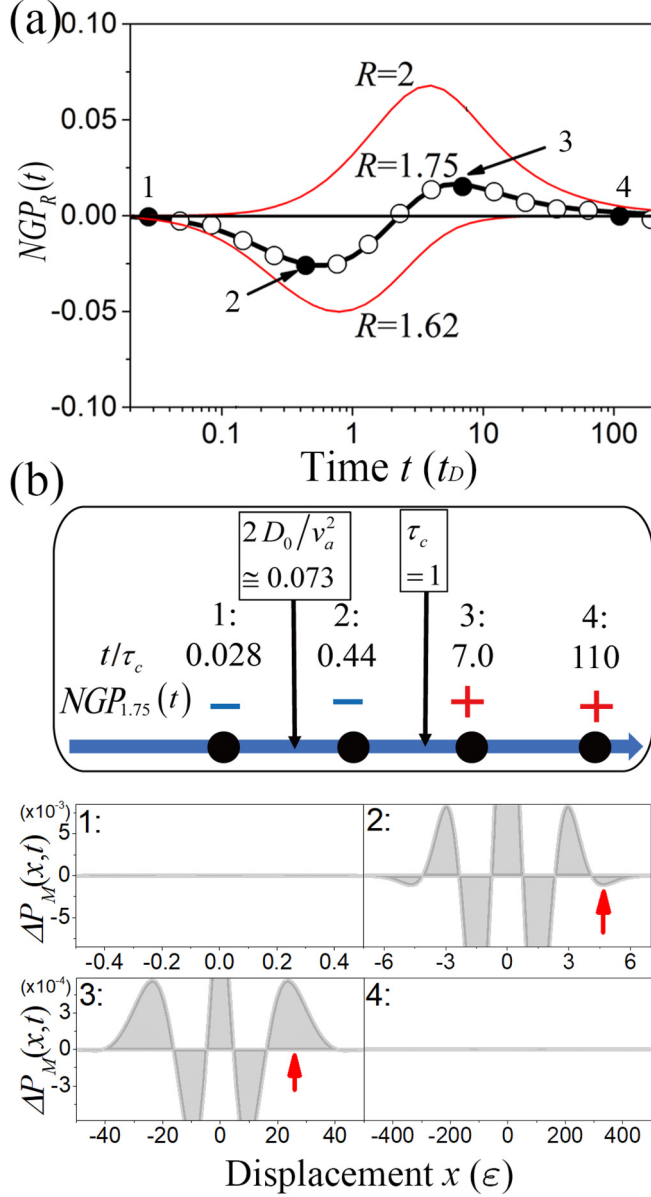


FIG. 4. Time evolution of displacement distribution from sub-Gaussian to super-Gaussian. When $1.62 < R < 2$, the displacement distribution of the multimode active matter model is sub-Gaussian at short times but super-Gaussian at long times. (a) $NGP_R(t)$ when $R = 1.75$: (lines) analytic results (circles) stochastic simulation results. The two red lines represent $NGP_R(t)$ for the two critical values of R , 1.62 and 2. (b) The deviation $\Delta P_M(x, t)$, of the displacement distributions, $P_M(x, t)$ from the Gaussian distribution with the same variance at the four different time points marked by the solid circles. $P_M(x, t)$ becomes Gaussian in the short- and the long-time limits. The red arrows indicate the tail peaks that determine the sign of the NGP value. The negative (positive) tail peak causes the NGP value to be negative (positive) at $t/t_D = 0.44(7.0)$. The length and time units are the same as in Fig. 2. The values of parameters used are $\tau_c = t_D$ and $D_a = 10D_0$.

times. The convergence of $NGP_{R,v_s}(t)$ to a constant value is consistent with Ref. [53]. At long times, $NGP_{R,v_s}(t)$ is proportional to t^{-1} and the ratio, $\langle x_{v_s}^2(t) \rangle / \langle x^2(t) \rangle^2$, approaches

a constant. This result explains the long-time behavior of $NGP_R(t)$.

For both of our models, the displacement distributions, $P_M(x, t)$ and $P_S(x, t)$, approach a Gaussian distribution at long times; however according to Eqs. (7) and (8), their deviation from Gaussian, measured by the non-Gaussian parameter, slowly decreases with time, following t^{-1} at long times ($t \gg \tau_c$). As shown in Fig. 3(c), the deviation of the displacement distribution from a Gaussian can be sizable even at long times where the MSD, given in Eq. (6), is linearly proportional to time. This result is consistent with the Fickian yet non-Gaussian diffusion of active matter observed in Refs. [2,5,58].

V. GENERALIZATION OF THEORETICAL MODEL

The multimode active matter model discussed above can be extended to a more complex model in a higher spatial dimension, d . For this generalized model, the stochastic differential equation corresponding to Eq. (1) is given by

$$\dot{\mathbf{r}}(t) = \mathbf{v}_{s,\Gamma}(t) + \gamma^{-1}\xi(t), \quad (10)$$

where each bold symbol denotes a d -dimensional vector corresponding to each scalar quantity in Eq. (1). The general expression of the MSD obtained from Eq. (10) is given by

$$\langle |\mathbf{r}(t)|^2 \rangle = 2d \int_0^t d\tau (t - \tau) [D_0 \tau_p^{-1} \phi_\xi(\tau) + D_a \tau_c^{-1} \phi_{v_s}(\tau)], \quad (11)$$

where D_0 , τ_p , D_a , and τ_c are, respectively, defined by $D_0 = d^{-1} \gamma^{-2} \int_0^\infty dt \langle \xi(t) \cdot \xi(0) \rangle$, $\tau_p \equiv \int_0^\infty dt \phi_\xi(t)$, $D_a = d^{-1} \int_0^\infty dt \langle \mathbf{v}_{s,\Gamma}(t) \cdot \mathbf{v}_{s,\Gamma}(0) \rangle$, and $\tau_c \equiv \int_0^\infty dt \phi_{v_s}(t)$. Here, $\phi_{v_s}(t)$ denotes the normalized time-correlation function, $\langle \mathbf{v}(t) \cdot \mathbf{v}(0) \rangle / \langle v(0)^2 \rangle$, of vector $\mathbf{v}(t)$. The functional form of $\phi_{v_s}(\tau)$ varies depending on the internal state dynamics and its coupling to the self-propelled velocity. Given that the relaxation time of random fluctuating force $\xi(t)$ is far shorter than the observation time t , Eq. (11) reduces to $\langle |\mathbf{r}(t)|^2 \rangle \cong 2dD_0t + 2dD_a\tau_c^{-1} \int_0^t d\tau (t - \tau) \phi_{v_s}(\tau)$. This result is the generalization of Eq. (6) for multidimensional systems with arbitrary $\phi_{v_s}(\tau)$; it reduces to Eq. (6) for the one-dimensional model with $\phi_{v_s}(\tau) = \exp(-\tau/\tau_c)$. In addition, the general expression of NGP can also be written as

$$NGP_R(t) = \frac{\langle |\mathbf{r}_{v_s}(t)|^2 \rangle^2}{\langle |\mathbf{r}(t)|^2 \rangle^2} NGP_{R,v_s}(t). \quad (12)$$

Here, $NGP_{R,v_s}(t)$ is defined by $NGP_{R,v_s}(t) \equiv \frac{d}{d+2} \langle |\mathbf{r}_{v_s}(t)|^4 \rangle / \langle |\mathbf{r}_{v_s}(t)|^2 \rangle^2 - 1$ with $\langle |\mathbf{r}_{v_s}(t)|^2 \rangle$ and $\langle |\mathbf{r}_{v_s}(t)|^4 \rangle$ defined as $\int_0^t \int_0^t d\tau_2 d\tau_1 \langle \mathbf{v}_{s,\Gamma}(\tau_2) \cdot \mathbf{v}_{s,\Gamma}(\tau_1) \rangle$ and $\int_0^t \int_0^t \int_0^t \int_0^t d\tau_4 d\tau_3 d\tau_2 d\tau_1 \langle \mathbf{v}_{s,\Gamma}(\tau_4) \cdot \mathbf{v}_{s,\Gamma}(\tau_3) \mathbf{v}_{s,\Gamma}(\tau_2) \cdot \mathbf{v}_{s,\Gamma}(\tau_1) \rangle$, respectively (see Appendix J). The NGP given in Eq. (12) vanishes in both the short-time and the long-time limits. At times far shorter than the relaxation timescale, τ_c , of self-propelled velocity, $(\langle |\mathbf{r}_{v_s}(t)|^2 \rangle / \langle |\mathbf{r}(t)|^2 \rangle)^2$ approaches zero, and hence $NGP_R(t)$ vanishes. On the other hand, in the long-time limit, $(\langle |\mathbf{r}_{v_s}(t)|^2 \rangle / \langle |\mathbf{r}(t)|^2 \rangle)^2$ approaches $(D_a / (D_0 + D_a))^2$, but $NGP_{R,v_s}(t)$, or the NGP of the self-propelled displacement, $\int_0^t d\tau \mathbf{v}_{s,\Gamma}(\tau)$, vanishes because its distribution becomes a Gaussian distribution, in accordance with the Gaussian

central limit theorem. However, the NGP has a nonzero value between the two limits. In the simple one-dimensional case, the multimode active matter model with Poisson state-switching dynamics, Eq. (12) reduces to Eq. (9). Equations (11) and (12) enable us to calculate the MSD and NGP for general multimode active matter with potentially non-Poisson state-switching dynamics.

VI. SUMMARY

We investigated the non-Gaussian character of the displacement distribution of multimode active matter that alternately undergoes passive diffusion and state-dependent self-propelled motion, examples of which are shown in Fig. 1. We find that the displacement distribution is always sub-Gaussian for the single-mode active matter that undergoes self-propelled motion only, shown in Fig. 1(a). However, for the multimode active matter shown in Fig. 1(b), the displacement distribution is super-Gaussian when the population ratio of the passive mode to the active modes is large but sub-Gaussian is small. For an intermediate range of the population ratio, the displacement distribution is sub-Gaussian at short times but super-Gaussian at longer times before it approaches Gaussian in the long-time limit. This non-Gaussian displacement distribution emerges even in timescales where the mean-square displacement exhibits the normal diffusion behavior. We also presented a generalization of our model to encompass a general multimode active matter in higher spatial dimensions.

ACKNOWLEDGMENTS

The authors are grateful to Mr. Dae Hyun Kim for helpful discussions and Mr. Luke Bates for his careful reading of our manuscript. This work was supported by the Creative Research Initiative Project program (Grant No. 2015R1A3A2066497) funded by the National Research Foundation (NRF) of Korea; the NRF grant (MSIT) (Grant No. 2020R1A5A1018052); the NRF grant (Grant No. 2017R1D1A1B03028457); and the Priority Research Center Program through the NRF (Grant No. 2009-0093817), funded by the Korean government.

APPENDIX A: DYNAMICS OF THE MULTIMODE ACTIVE MATTER MODEL

For the multimode active matter model, the velocity of the self-propelled motion of an active particle is dependent on the internal state, Γ , of the active matter. In the high-friction regime, we specify the state of our active matter by its position, x , and the internal state, Γ , of active matter. In this work, we consider only active matter with discrete internal states, $\{\Gamma_i\}$. Assuming the dynamics of x and Γ_i is a multidimensional Markov process, one can obtain the time-evolution equation governing the joint probability density function, $P(\Gamma_i, x, t)$, of the active matter state, starting from the following generalized Chapman-Kolmogorov equation [59]:

$$P(\Gamma_i, x, t + \Delta t) = \int d(\Delta x) P(\Gamma_i, x - \Delta x, t) \Psi(x - \Delta x; \Delta x) + \sum_j [P(\Gamma_j, x, t) T_{j \rightarrow i} - P(\Gamma_i, x, t) T_{i \rightarrow j}], \quad (\text{A1})$$

where $\Psi(x; \Delta x)$ and $T_{j \rightarrow i}$ denote the probability that x undergoes a change Δx in time interval Δt and the probability of transition from state Γ_j to state Γ_i in time interval Δt , respectively. Using the Taylor series expansions of Eq. (A1), we obtain

$$\begin{aligned} \frac{\partial P(\Gamma_i, x, t)}{\partial t} \Delta t + O(\Delta t^2) = & -\frac{\partial}{\partial x} [\langle \Delta x \rangle P(\Gamma_i, x, t)] + \frac{1}{2} \frac{\partial^2}{\partial x^2} [\langle \Delta x^2 \rangle P(\Gamma_i, x, t)] \\ & + \sum_j \{P(\Gamma_j, x, t) K_{j \rightarrow i} - P(\Gamma_i, x, t) K_{i \rightarrow j}\} \Delta t + O(\Delta t^2), \end{aligned} \quad (\text{A2})$$

where $\langle \Delta x^k \rangle$ and $K_{j \rightarrow i}$ are defined by $\langle \Delta x^k \rangle = \int d(\Delta x) \Delta x^k \Psi(x; \Delta x)$ and $T_{j \rightarrow i} = K_{j \rightarrow i} \Delta t + O(\Delta t^2)$, respectively.

The expressions of $\langle \Delta x \rangle$ and $\langle \Delta x^2 \rangle$ in Eq. (A2) can be obtained from the Langevin equation describing stochastic motion of our active matter model in the high-friction regime, i.e.,

$$\gamma v(t) \cong F(\Gamma) + \xi(t), \quad (\text{A3})$$

where γ , $v(t)$, $F(\Gamma)$, and $\xi(t)$, respectively, denote the friction coefficient, the velocity of active matter at time t , the force associated with the self-propelled motion of active matter at state Γ , and the random and rapidly fluctuating force. By integrating Eq. (A3) over time from t to $t + \Delta t$, we obtain

$$\Delta x[\equiv x(t + \Delta t) - x(t)] = \gamma^{-1} \left[F(\Gamma) \Delta t + \int_t^{t+\Delta t} \xi(\tau) d\tau \right]. \quad (\text{A4})$$

In obtaining Eq. (A4), we assume that the change in F during time interval Δt is negligible. By taking average of Eq. (A4) over the entire realization of stochastic processes, $\{\Gamma(t), \xi(t)\}$, and by assuming that the random fluctuation force has an isotropic distribution, $\langle \xi(t) \rangle = 0$, we obtain

$$\langle \Delta x \rangle = v_s(\Gamma) \Delta t + O(\Delta t^2), \quad (\text{A5})$$

where $v_s(\Gamma)$ is defined by $F(\Gamma)/\gamma$. From Eq. (A4), one can also obtain the following expression for $\langle \Delta x^2 \rangle$:

$$\langle \Delta x^2 \rangle = \gamma^{-2} \int_t^{t+\Delta t} d\tau_2 \int_t^{\tau_2} d\tau_1 \langle \xi(\tau_2)\xi(\tau_1) \rangle + O(\Delta t^2), \quad (\text{A6})$$

which follows because the random fluctuating force is not correlated with the state-dependent force, i.e., $\langle F(\Gamma(t))\xi(t) \rangle = 0$. Substituting the well-known fluctuation-dissipation relation, $\langle \xi(\tau_2)\xi(\tau_1) \rangle = 2\gamma k_B T \delta(\tau_2 - \tau_1)$, into Eq. (A6), we obtain

$$\langle \Delta x^2 \rangle = \frac{2k_B T}{\gamma} \Delta t + O(\Delta t^2). \quad (\text{A7})$$

By substituting Eqs. (A5) and (A7) into Eq. (A2), we obtain

$$\frac{\partial P(\Gamma_i, x, t)}{\partial t} = -\frac{\partial}{\partial x} [v_s(\Gamma)P(\Gamma_i, x, t)] + \frac{k_B T}{\gamma} \frac{\partial^2}{\partial x^2} P(\Gamma_i, x, t) + \sum_j \{P(\Gamma_j, x, t)K_{j \rightarrow i} - P(\Gamma_i, x, t)K_{i \rightarrow j}\} \quad (\text{A8})$$

Identifying $D = k_B T/\gamma$, we obtain Eq. (2) in the main text from Eq. (A8).

APPENDIX B: DERIVATION OF THE SECOND AND FOURTH MOMENTS OF DISPLACEMENT FOR THE MULTIMODE MODEL

The multimode active matter model has three internal states, Γ_+ , Γ_0 , and Γ_- . Each internal state regulates the direction and speed of a given active matter as depicted in Fig. 1(b), based on the initial conditions that the internal states are initially in equilibrium and the initial position of active matter is zero. Three simultaneous equations are obtained from Eq. (4) by applying the Fourier transform and the Laplace transform to $P_i(x, t)$ with $i \in +, 0, -$. The solution of the simultaneous equations provides three probability density functions for the individual internal states in the Fourier-Laplace domain, written as

$$\begin{pmatrix} \tilde{P}_+(w, s) \\ \tilde{P}_0(w, s) \\ \tilde{P}_-(w, s) \end{pmatrix} = \frac{1}{(s + D_0 w^2)(\chi(w, s) + v_a^2 w^2) + 2k_{0a} v_a^2 w^2} \begin{pmatrix} p_+^{eq}(\chi(w, s) - i v_a w(s + D_0 w^2 + k_{a0} + 2k_{0a})) \\ p_0^{eq}(\chi(w, s) + v_a^2 w^2) \\ p_-^{eq}(\chi(w, s) + i v_a w(s + D_0 w^2 + k_{a0} + 2k_{0a})) \end{pmatrix} \quad \text{with} \quad (\text{B1})$$

$$\chi(w, s) \equiv (s + D_0 w^2 + k_{a0})(s + D_0 w^2 + k_{a0} + 2k_{0a}).$$

In Eq. (B1), w and s , respectively, denote the Fourier transform of position x and the Laplace transform of time t . The tildes indicate that the functions are represented in the Fourier-Laplace domain. p_+^{eq} , p_0^{eq} , and p_-^{eq} denote the equilibrium probabilities of the states Γ_+ , Γ_0 , and Γ_- , respectively. A summation of the PDFs, given in Eq. (B1), provides the PDF of multimode active matter, which is given by

$$\tilde{P}_M(w, s) \equiv \tilde{P}_-(w, s) + \tilde{P}_0(w, s) + \tilde{P}_+(w, s) = \frac{\chi(w, s) + p_0^{eq} v_a^2 w^2}{(s + D_0 w^2)(\chi(w, s) + v_a^2 w^2) + 2k_{0a} v_a^2 w^2}. \quad (\text{B2})$$

The denominator in Eq. (B2) is a cubic function of $z \equiv s + D_0 w^2$ as $z^3 + 2(k_{a0} + k_{0a})z^2 + (k_{a0}(k_{a0} + 2k_{0a}) + v_a^2 w^2)z + 2k_{0a} v_a^2 w^2$. If we assume the roots of the cubic function as $-C_i(w)$ with ($i = 1, 2, 3$), the PDF can be rewritten as

$$\begin{aligned} \tilde{P}_M(w, s) &= \frac{1}{s + D_0 w^2} - 2k_{0a} v_a^2 w^2 \left(\frac{1}{s + D_0 w^2} + \frac{1}{k_{a0} + 2k_{0a}} \right) \prod_{i=1}^3 \frac{1}{s + D_0 w^2 + C_i(w)} \\ &= \frac{1}{s + D_0 w^2} - 2k_{0a} v_a^2 w^2 \left(\frac{1}{s + D_0 w^2} + \frac{1}{k_{a0} + 2k_{0a}} \right) \sum_{i=1}^3 \frac{1}{s + D_0 w^2 + C_i(w)} \prod_{j \neq i}^3 \frac{1}{C_i(w) - C_j(w)}. \end{aligned} \quad (\text{B3})$$

Inverting s in $\tilde{P}(w, s)$ generates the Fourier domain PDF, written as

$$\hat{P}_M(w, t) = v_a^2 w^2 e^{-D_0 w^2 t} \left(\sum_{i=1}^3 \left(\frac{2k_{0a}}{C_i(w)} - \frac{2k_{0a}}{k_{a0} + 2k_{0a}} \right) e^{-C_i(w)t} \prod_{j \neq i}^3 \frac{1}{C_i(w) - C_j(w)} \right). \quad (\text{B4})$$

Equations (B2) and (B4) can both be used to derive the analytic solution for the MSD of the multimode model. One way is to use the second partial derivative of $\hat{P}_M(w, t)$, while the other way, which is an easier way to obtain the time-domain MSD, is to apply the inverse Laplace transform to the second partial derivative of $\tilde{P}_M(w, s)$, written as

$$\langle x^2(t) \rangle = \lim_{w \rightarrow 0} \left[-\frac{\partial^2 \hat{P}_M(w, t)}{\partial w^2} \right] = L_{s \rightarrow t}^{-1} \left(\lim_{w \rightarrow 0} \left[-\frac{\partial^2 \tilde{P}_M(w, s)}{\partial w^2} \right] \right) = 2D_0 t + 2D_a \tau_c (e^{-t/\tau_c} - 1 + t/\tau_c), \quad (\text{B5})$$

where $L_{s \rightarrow t}^{-1}$ and D_α denote the inverse Laplace transform operator and $D_a \equiv \int_0^\infty dt \langle v_s(t) v_s(0) \rangle = \tau_c v_a^2 p_a$ with p_a being the probability of active states, $p_a = 2k_{0a}/(k_{a0} + 2k_{0a})$. The time-dependent MSD of this model is given in Eq. (6).

The analytic solution for the fourth moment of the displacement is obtained using the following equation:

$$\langle x^4(s) \rangle = \lim_{w \rightarrow 0} \left[\frac{\partial^4 \tilde{P}_M(w, s)}{\partial w^4} \right] = \frac{24}{s^3} \left[D_0^2 + \frac{2v_a^2 k_{0a}}{(s + k_{a0})(k_{a0} + 2k_{0a})} \left(3D_0 - \frac{1}{s + k_{a0}} \left(k_{a0} D_0 - v_a^2 + \frac{v_a^2 k_{a0}}{s + k_{a0} + 2k_{0a}} \right) \right) \right]. \quad (\text{B6})$$

Applying the inverse Laplace transform to Eq. (B6) provides the fourth moment of displacement in the time domain, written as

$$\begin{aligned} \langle x^4(t) \rangle = & 12(D_0 + D_a)^2 t^2 + \frac{24D_a^2 \tau_c^2}{(R+1)^2} (R^5 e^{-(1+1/R)t/\tau_c} + (-R^2 + 3R - 3)(R+1)^3 e^{-t/\tau_c} - (3R^3 - R^2 - 6R - 3) \\ & + (R+1)^2 (R^2 - 1 + D_0/D_a) e^{-t/\tau_c} t/\tau_c + (R+1)(R^2 - 2R - 2 - (R+1)D_0/D_a) t/\tau_c. \end{aligned} \quad (\text{B7})$$

The second and fourth moments expressed in the time domain are combined to produce the NGP:

$$\begin{aligned} \text{NGP}_R(t) \equiv & \frac{\langle x^4(t) \rangle}{3\langle x^2(t) \rangle^2} - 1 = \frac{1}{3} \kappa(t) - 1 \\ = & \frac{1}{(R+1)^4} \left(\frac{2D_a^{(0)} \tau_c}{\langle x^2(t) \rangle} \right)^2 \left(-e^{-2t/\tau_c} - 4e^{-t/\tau_c} + 5 - 4e^{-t/\tau_c} t/\tau_c - 2t/\tau_c + (-2e^{-2t/\tau_c} - 8e^{-t/\tau_c} + 10 - 8e^{-t/\tau_c} t/\tau_c - 4t/\tau_c) R \right. \\ & \left. + (-e^{-2t/\tau_c} + 1 - 2e^{-t/\tau_c} t/\tau_c) R^2 + (6e^{-t/\tau_c} - 6 + 4e^{-t/\tau_c} t/\tau_c + 2t/\tau_c) R^3 + 2 \left(e^{-(1/R)t/\tau_c} - 1 + \frac{1}{R} t/\tau_c \right) e^{-t/\tau_c} R^5 \right) \end{aligned}$$

with

$$\frac{\langle x^2(t) \rangle}{2D_a^{(0)} \tau_c} = \frac{D_0}{D_a^{(0)}} \frac{t}{\tau_c} + \frac{1}{(R+1)} \left(e^{-t/\tau_c} + \frac{t}{\tau_c} - 1 \right), \quad (\text{B8})$$

where $\kappa(t)$ denotes kurtosis and $D_a^{(0)} \equiv (R+1)D_a = \tau_c v_a^2$. On the log-scale time axis, as shown in Fig. 3(b), the relaxation time, τ_c , shifts the $\text{NGP}_R(t)$ curve along the time axis as well as the MSD curve. In Fig. 3(d), $\text{NGP}_R(t)$ in all ranges of R and t/τ_c is evaluated and plotted under the condition that $D_0/D_a^{(0)} = 0.1$, where the red lines are the two lines shown in Fig. 3(c) and the black line marks a border line switching from sub-Gaussian to super-Gaussian at a given R . Although $\text{NGP}_R(t)$ depends on $D_0/D_a^{(0)}$, the border line is invariant to the change of the $D_0/D_a^{(0)}$ ratio in Eq. (B8). Thus, $\text{NGP}_R(t)$ with R less than $(1 + \sqrt{5})/2$ is sub-Gaussian at all times, and $\text{NGP}_R(t)$ with R larger than 2 is super-Gaussian at all times. When $(1 + \sqrt{5})/2 < R < 2$, $P_M(x, t)$ can switch from sub-Gaussian to super-Gaussian over time, as shown in Fig. 4(a).

APPENDIX C: DERIVATION OF THE SECOND AND FOURTH MOMENTS OF DISPLACEMENT FOR THE SINGLE-MODE MODEL

The single-mode model has two internal states, Γ_+ and Γ_- . Each internal state regulates the direction and speed of active matter, as shown in Fig. 1(a). Based on the initial conditions that the internal states are initially in equilibrium and the initial position of active matter is zero, two simultaneous equations are obtained from Eq. (3) by applying the Fourier transform and the Laplace transform to $P_i(x, t)$ with $i \in +, -$. The analytic solution of the simultaneous equations provides two PDFs in the Fourier-Laplace domain, written as

$$\begin{pmatrix} \tilde{P}_+(w, s) \\ \tilde{P}_-(w, s) \end{pmatrix} = \frac{1}{2} \frac{1}{v_a^2 w^2 + (s + D_0 w^2)(s + D_0 w^2 + 2k_{aa})} \begin{pmatrix} s + D_0 w^2 + 2k_{aa} - i v_a w \\ s + D_0 w^2 + 2k_{aa} + i v_a w \end{pmatrix}. \quad (\text{C1})$$

The PDF of active matter for the single-mode model in Fourier-Laplace domain is written as

$$\tilde{P}_S(w, s) \equiv \tilde{P}_-(w, s) + \tilde{P}_+(w, s) = \frac{s + D_0 w^2 + 2k_{aa}}{v_a^2 w^2 + (s + D_0 w^2)(s + D_0 w^2 + 2k_{aa})}. \quad (\text{C2})$$

Applying the inverse Laplace transform to Eq. (C2) generates the PDF of active matter represented in the Fourier domain as

$$\hat{P}_S(w, t) = e^{-t(k_{aa} + D_0 w^2)} \left(\cosh(t \Lambda) + \frac{k_{aa}}{\Lambda} \sinh(t \Lambda) \right) \quad \text{with} \quad \Lambda \equiv \sqrt{k_{aa}^2 - v_a^2 w^2}. \quad (\text{C3})$$

From this function, the time-dependent second and fourth moments of displacement are simple to obtain. The time-dependent MSD of this model is given in Eq. (6). The fourth moment of displacement is also evaluated from the PDF as

$$\langle x^4(t) \rangle = 12\tau_c^2 \left((D_0 + D_a)^2 \frac{t^2}{\tau_c^2} + 2D_a \left((D_a - D_0)(1 - e^{-t/\tau_c}) \frac{t}{\tau_c} + 3D_a \left(1 - e^{-t/\tau_c} - \frac{t}{\tau_c} \right) \right) \right), \quad (\text{C4})$$

where $D_a = \tau_c v_a^2$. The second and fourth moments expressed in the time domain can be combined to produce the NGP:

$$\text{NGP}_0(t) = \left(\frac{2D_a \tau_c}{\langle x^2(t) \rangle} \right)^2 (5 - e^{-2t/\tau_c} - 4e^{-t/\tau_c} - 4e^{-t/\tau_c} t/\tau_c - 2t/\tau_c) = \left(\frac{2D_a \tau_c}{\langle x^2(t) \rangle} \right)^2 \beta(t)$$

with

$$\frac{\langle x^2(t) \rangle}{2D_a \tau_c} = \frac{D_0 t}{D_a \tau_c} + \left(e^{-t/\tau_c} + \frac{t}{\tau_c} - 1 \right)$$

and

$$\beta(t) \equiv 5 - e^{-2t/\tau_c} - 4e^{-t/\tau_c} - 4e^{-t/\tau_c} t/\tau_c - 2t/\tau_c. \quad (\text{C5})$$

In Eq. (C5), $\text{NGP}_0(t)$ is less than or equal to zero because $\beta(t) \leq 0$ in all time ranges, and the equation is equal to $\text{NGP}_R(t)$ of the multimode model in the small- R limit as $\text{NGP}_0(t) = \lim_{R \rightarrow 0} \text{NGP}_R(t)$.

APPENDIX D: TIME-CORRELATION FUNCTIONS FOR TWO MODELS

Time-correlation functions of the velocity component, v_s , of self-propelled motion are used to calculate D_a and $\text{NGP}_R(t)$ as well as the second and fourth moments of displacement. In our model, because v_s is only dependent on the internal state, we analytically obtain the time evolution of internal state probabilities as

$$\begin{pmatrix} P_+(t) \\ P_-(t) \end{pmatrix} = \mathbf{G} \begin{pmatrix} P_+(0) \\ P_-(0) \end{pmatrix} \quad \text{with} \quad \mathbf{G} = e^{-k_{aa}t} \begin{pmatrix} \cosh(k_{aa}t) & \sinh(k_{aa}t) \\ \sinh(k_{aa}t) & \cosh(k_{aa}t) \end{pmatrix} \quad (\text{D1})$$

for the single-mode model and

$$\begin{pmatrix} P_+(t) \\ P_0(t) \\ P_-(t) \end{pmatrix} = \mathbf{G}(t) \begin{pmatrix} P_+(0) \\ P_0(0) \\ P_-(0) \end{pmatrix}$$

with

$$\mathbf{G}(t) = \frac{1}{k} \begin{pmatrix} k_{0a} + \frac{k_{a0}e^{-kt} + ke^{-k_{a0}t}}{2} & k_{0a} - k_{0a}e^{-kt} & k_{0a} + \frac{k_{a0}e^{-kt} - ke^{-k_{a0}t}}{2} \\ k_{a0} - k_{a0}e^{-kt} & k_{a0} + 2k_{0a}e^{-kt} & k_{a0} - k_{a0}e^{-kt} \\ k_{0a} + \frac{k_{a0}e^{-kt} - ke^{-k_{a0}t}}{2} & k_{0a} - k_{0a}e^{-kt} & k_{0a} + \frac{k_{a0}e^{-kt} + ke^{-k_{a0}t}}{2} \end{pmatrix}$$

and

$$k \equiv k_{a0} + 2k_{0a} \quad (\text{D2})$$

for the multimode model. We obtain the velocity autocorrelation function, $\langle \mathbf{v}_s(t) \cdot \mathbf{v}_s(0) \rangle$, through the following equation:

$$\langle v_s(t) v_s(0) \rangle = \sum_{i \in +, -} \sum_{j \in +, -} v_s(\Gamma_j) v_s(\Gamma_i) \mathbf{G}(t)_{ji} P(\Gamma_i, 0), \quad (\text{D3})$$

where $\mathbf{G}(t)_{ji}$ denotes a transition matrix from Γ_i to Γ_j after t time passing. The transition matrices are shown in Eq. (D1) for the single-mode model and in Eq. (D2) for the multimode model. The calculation results of $\langle v_s(t) v_s(0) \rangle$ are $v_a^2 e^{-2k_{aa}t}$ for the single-mode model and $p_a v_a^2 e^{-k_{a0}t}$ for the multimode model. The four-time velocity autocorrelation function, $\langle v_s(t_4) v_s(t_3) v_s(t_2) v_s(t_1) \rangle$, is obtained by the following equation, written as

$$\langle v_s(t_4) v_s(t_3) v_s(t_2) v_s(t_1) \rangle = \sum_{i \in +, -} \sum_{j \in +, -} \sum_{k \in +, -} \sum_{l \in +, -} v_s(\Gamma_l) v_s(\Gamma_k) v_s(\Gamma_j) v_s(\Gamma_i) \mathbf{G}(t_4 - t_3)_{lk} \mathbf{G}(t_3 - t_2)_{kj} \mathbf{G}(t_2 - t_1)_{ji} P(\Gamma_i, t_1). \quad (\text{D4})$$

The results of $\langle v_s(t_4) v_s(t_3) v_s(t_2) v_s(t_1) \rangle$ are $v_a^4 e^{-2k_{aa}(t_4 - t_3 + t_2 - t_1)}$ for the single-mode model and $p_a^2 v_a^4 (e^{k_{a0}(t_3 - t_2)} + \mathbb{R} e^{-2k_{0a}(t_3 - t_2)}) e^{-k_{a0}(t_4 - t_1)}$ for the multimode model. The four-time velocity autocorrelation functions can be used to generate $\langle |\mathbf{r}_{\mathbf{v}_s}(t)|^4 \rangle$ in Eq. (J4), and their results are equal to the fourth moment of displacement written in Eqs. (B7) and (C4).

APPENDIX E: RELAXATION TIME OF THE TWO MODELS

In the high-friction regime, where we can safely neglect the inertial term in the Langevin equation, the velocity, $\dot{x}(t)$, of active matter with a friction constant, γ , can be written as the sum of two components:

$$\dot{x}(t) = v_s(t) + \gamma^{-1} \xi(t), \quad (\text{E1})$$

where $v_s(t)$ and $\gamma^{-1} \xi(t)$ represent the velocity component of self-propelled, ballistic motion and the velocity component caused by random fluctuating force. If we assume that the initial position of active matter is zero, then the time integration of Eq. (E1)

produces the time-dependent position, written as

$$x(t) = \int_0^t (v_s(\tau) + \gamma^{-1}\xi(\tau))d\tau. \quad (\text{E2})$$

From Eq. (E2), the MSD of the active matter can be evaluated from the velocity correlation function, written as

$$\begin{aligned} \langle x^2(t) \rangle &= \int_0^t d\tau_2 \int_0^t d\tau_1 \left[\langle v_s(\tau_2)v_s(\tau_1) \rangle + \frac{1}{\gamma^2} \langle \xi(\tau_2)\xi(\tau_1) \rangle \right] \\ &= 2D_0t + 2 \int_0^t d\tau (t - \tau) \langle v_s(\tau)v_s(0) \rangle. \end{aligned} \quad (\text{E3})$$

By comparing Eq. (E3) with Eq. (6), we obtain the following equation:

$$\int_0^t d\tau (t - \tau) \langle v_s(\tau)v_s(0) \rangle = D_a \tau_c (e^{-t/\tau_c} - 1 + t/\tau_c). \quad (\text{E4})$$

Because D_a is equal to $\tau_c \langle v_s^2 \rangle$, the second derivative of each side of Eq. (E4) provides the normalized time-correlation function of velocity, $\phi_{v_s}(t)$, as

$$\phi_{v_s}(t) = \langle v_s(t)v_s(0) \rangle / \langle v_s^2 \rangle = e^{-t/\tau_c}, \quad (\text{E5})$$

where the comparison result of τ_c is given by $(2k_{aa})^{-1}$ for the single-mode model and k_{a0}^{-1} for the multimode model which is consistent with Eq. (D3).

APPENDIX F: PROBABILITY DENSITY FUNCTION OF THE DISPLACEMENT AT SHORT AND LONG TIMES

The diffusion dynamics of our models is highly dependent on the relaxation time, τ_c , of the velocity, $v_s(\Gamma)$. At short times ($t \ll \tau_c$), a given active matter maintains its direction and magnitude of velocity, and each unrelaxed velocity produces three individual peaks in the PDF of displacement. The PDF of displacement at short times is derived from Eq. (B1), which is written as

$$\begin{pmatrix} \tilde{P}_{\text{short},+}(w, s) \\ \tilde{P}_{\text{short},0}(w, s) \\ \tilde{P}_{\text{short},-}(w, s) \end{pmatrix} = \begin{pmatrix} p_+^{eq}(s + D_0w^2 + i v_a w)^{-1} \\ p_0^{eq}(s + D_0w^2)^{-1} \\ p_-^{eq}(s + D_0w^2 - i v_a w)^{-1} \end{pmatrix}. \quad (\text{F1})$$

$P_M(x, t)$ at short times is written as

$$P_{M,\text{short}}(x, t) = \frac{1}{\sqrt{4\pi D_0 t}} \left(p_-^{eq} e^{-[(x+v_a t)^2/4D_0 t]} + p_0^{eq} e^{-(x^2/4D_0 t)} + p_+^{eq} e^{-[(x-v_a t)^2/4D_0 t]} \right), \quad (\text{F2})$$

where the distribution is a Gaussian with a variance of $2D_0t$. The three peaks in $P_{M,\text{short}}(x, t)$ are approximated as a single Gaussian function with a small variance at very short times ($t \ll 2D_0/v_a^2$) that gradually separate as time increases.

At long times ($t \gg \tau_c$), the peaks of individual $v_s(\Gamma)$ s are again intermingled into a single Gaussian and follow the distribution, written as

$$\begin{pmatrix} \tilde{P}_{\text{long},+}(w, s) \\ \tilde{P}_{\text{long},0}(w, s) \\ \tilde{P}_{\text{long},-}(w, s) \end{pmatrix} = \frac{1}{s + D_{\text{eff}}w^2} \begin{pmatrix} p_+^{eq}(1 - i v_a w/k_{a0}) \\ p_0^{eq}(1 + v_a^2 w^2/k_{a0}(k_{a0} + 2k_{0a})) \\ p_-^{eq}(1 + i v_a w/k_{a0}) \end{pmatrix}, \quad (\text{F3})$$

where D_{eff} is equal to $D_0 + D_a$. The PDF $P_M(x, t)$ at long times is written as

$$P_{M,\text{long}}(x, t) = \frac{1}{\sqrt{4\pi D_{\text{eff}} t}} e^{-(x^2/4D_{\text{eff}} t)} \left(1 + \frac{p_0^{eq} D_a \tau_c R}{2D_{\text{eff}} t} \left(1 - \frac{x^2}{2D_{\text{eff}} t} \right) \right). \quad (\text{F4})$$

In Eq. (F4), the deviation from Gaussian is proportional to $p_0^{eq} D_a \tau_c R / 2D_{\text{eff}} t$. Thus, at long times, $P_M(x, t)$ approaches a Gaussian distribution in accordance with the central limit theorem.

APPENDIX G: MEAN VELOCITY DISTRIBUTION AND STATIONARY DISTRIBUTION

The mean velocity, $\bar{v}(t)$, is defined by $\bar{v}(t) \equiv x(t)/t$. The mean velocity distribution, $f(\bar{v}, t)$, is related to the probability density function $p(x, t)$ of displacement by $P(x, t) = t^{-1} f(\bar{v} \equiv x/t, t)$. From the short-time expression of the displacement PDF in Eq. (F2), we obtain the following expression of the short-time mean velocity distribution of our multimode active matter model:

$$f_{M,\text{short}}(\bar{v}, t) = \frac{1}{\sqrt{4\pi D_0 t}} \left(p_-^{eq} e^{-[(\bar{v}+v_a)^2/(4D_0 t)]} + p_0^{eq} e^{-[\bar{v}^2/(4D_0 t)]} + p_+^{eq} e^{-[(\bar{v}-v_a)^2/(4D_0 t)]} \right) \quad (t \ll \tau_c). \quad (\text{G1})$$

The short-time mean velocity distribution is the sum of three Gaussian functions with the same variance, $2D_0/t$, which are centered at v_a , 0, and $-v_a$. Because the variance is inversely proportional to t , the width of the individual peaks in Eq. (G1) decreases over time. Note that, in the small- t limit, the variance of the mean velocity diverges. This follows because, in our model, active matter motion occurs under random fluctuating force modeled as Gaussian white noise. The mean velocity, x/t , approaches the instantaneous velocity in the small- t limit, which obeys our Langevin equation (1) in the main text. In Eq. (1), the variance of Gaussian white noise, $\xi(t)$, is infinite at all times, and so too is the variance of the instantaneous velocity.

On the other hand, at long times ($t \gg \tau_c$), $f_M(\bar{v}, t)$ takes the following form:

$$f_{M,\text{long}}(\bar{v}, t) = \frac{1}{\sqrt{4\pi D_{\text{eff}}/t}} e^{-[\bar{v}^2/(4D_{\text{eff}}/t)]} \left(1 + \frac{p_0^{\text{eq}} D_a \tau_c R}{2D_{\text{eff}} t} \left(1 - \frac{\bar{v}^2}{2D_{\text{eff}}/t} \right) \right). \quad (\text{G2})$$

Note that $f_{M,\text{long}}(\bar{v}, t)$ approaches the delta function centered at 0 in the long-time limit.

APPENDIX H: DERIVATION OF SHORT-TIME MEAN VELOCITY DISTRIBUTION FROM EQ. (1)

In our model, the velocity of active matter consists of two components in Eq. (1). If we assume that the two components are independent, then the mean velocity distribution is written as

$$f(\bar{v}, t) = \int dv_s dv_\xi \delta(\bar{v} - (v_s + v_\xi)) f_s(v_s, t) f_\xi(v_\xi, t), \quad (\text{H1})$$

where v_s and $f_s(v_s, t)$, respectively, denote the velocity component caused by self-propelled motion and its distribution function; $v_\xi [\equiv \gamma^{-1} \xi(t)]$ and $f_\xi(v_\xi, t)$ denote the velocity component due to the random fluctuating force and its distribution function. At short times, the velocity component, v_ξ , caused by the random fluctuating force is already relaxed and follows a Gaussian distribution with a variance of $2D_0/t$, whereas the self-propelled motion approximately maintains its direction. The two distribution functions at short times can be written as

$$f_\xi(v_\xi, t) = e^{-[v_\xi^2/(4D_0/t)]} / \sqrt{4\pi D_0/t} \quad \text{and} \quad f_s(v_s, t) = \sum_{i \in \Gamma} p_i^{\text{eq}} \delta(v_s - v_i). \quad (\text{H2})$$

By applying Eq. (H2) to Eq. (H1), the mean velocity distribution function at short times can be rewritten as

$$\begin{aligned} f_{\text{short}}(\bar{v}, t) &= \frac{1}{2\pi} \int_{-\infty}^{\infty} du \int dv_s dv_\xi e^{iu(\bar{v} - (v_s + v_\xi))} \sum_{i \in \Gamma} p_i^{\text{eq}} \delta(v_s - v_i) f_\xi(v_\xi, t) \\ &= \frac{1}{2\pi} \sum_{i \in \Gamma} p_i^{\text{eq}} \int_{-\infty}^{\infty} du e^{iu(\bar{v} - v_i)} \int dv_\xi e^{-iuv_\xi} f_\xi(v_\xi, t) \\ &= \sum_{i \in \Gamma} p_i^{\text{eq}} \int dv_\xi f_\xi(v_\xi, t) \delta(\bar{v} - v_i - v_\xi) = \sum_{i \in \Gamma} p_i^{\text{eq}} f_\xi(\bar{v} - v_i, t) \\ &= \sum_{i \in \Gamma} p_i^{\text{eq}} \frac{1}{\sqrt{4\pi D_0/t}} e^{-[(\bar{v} - v_i)^2/(4D_0/t)]}. \end{aligned} \quad (\text{H3})$$

Here, Eq. (H3) is equivalent to Eq. (G1), which is shown in Eq. (5).

APPENDIX I: CONVERGENCE OF $P_M(x, t)$ TO $P_S(x, t)$ AT THE SMALL- R LIMIT

The population ratio, $R (\equiv p_0^{\text{eq}} / (p_+^{\text{eq}} + p_-^{\text{eq}}) = \tau_0 / \tau_a = k_{a0} / 2k_{0a})$, of the passive state to the active state modulates the shape of the probability density of active matter, $P_M(x, t)$, in the multimode model. Applying $k_{a0} = \tau_c^{-1}$ and $2k_{0a} = R^{-1} \tau_c^{-1}$ to Eq. (B2) produces $\tilde{P}_M(w, s)$, written as

$$\begin{aligned} \tilde{P}_M(w, s) &= \frac{(s + D_0 w^2 + \tau_c^{-1})(s + D_0 w^2 + \tau_c^{-1} + R^{-1} \tau_c^{-1}) + v_a^2 w^2 R / (R + 1)}{(s + D_0 w^2)((s + D_0 w^2 + \tau_c^{-1})(s + D_0 w^2 + \tau_c^{-1} + R^{-1} \tau_c^{-1}) + v_a^2 w^2) + R^{-1} \tau_c^{-1} v_a^2 w^2} \\ &= \frac{(s + D_0 w^2 + \tau_c^{-1})(Rs + RD_0 w^2 + R\tau_c^{-1} + \tau_c^{-1}) + v_a^2 w^2 R^2 / (R + 1)}{(s + D_0 w^2)((s + D_0 w^2 + \tau_c^{-1})(Rs + RD_0 w^2 + R\tau_c^{-1} + \tau_c^{-1}) + Rv_a^2 w^2) + \tau_c^{-1} v_a^2 w^2}. \end{aligned} \quad (\text{I1})$$

In the limit of $R \rightarrow 0$, $\tilde{P}_M(w, s)$ in Eq. (I1) reduces to

$$\lim_{R \rightarrow 0} \tilde{P}_M(w, s) = \frac{s + D_0 w^2 + \tau_c^{-1}}{(s + D_0 w^2)(s + D_0 w^2 + \tau_c^{-1}) + v_a^2 w^2}. \quad (\text{I2})$$

Because the relaxation time of the single-mode model is $\tau_c = (2k_{aa})^{-1}$, applying $2k_{aa} = \tau_c^{-1}$ to Eq. (C2) produces $\tilde{P}_S(w, s)$:

$$\tilde{P}_S(w, s) = \frac{s + D_0 w^2 + \tau_c^{-1}}{(s + D_0 w^2)(s + D_0 w^2 + \tau_c^{-1}) + v_a^2 w^2}. \quad (I3)$$

$\tilde{P}_S(w, s)$ is the same as $\tilde{P}_M(w, s)$ in the small- R limit. This derivation also proves that $f_M(\bar{v}, t)$ approaches $f_S(\bar{v}, t)$ in the small- R limit.

APPENDIX J: GENERAL MODEL

In general, active matter moves in a multidimensional space, d , and its random fluctuating force has a finite relaxation time, τ_p . To obtain analytic solutions for this general model, the velocity of active matter corresponding to Eq. (1) is generalized to

$$\dot{\mathbf{r}}(t) = \mathbf{v}_s(t) + \gamma^{-1} \xi(t), \quad (J1)$$

where each bold symbol denotes a d -dimensional vector corresponding to each scalar quantity in Eq. (1). The integration of each side of Eq. (J1) from 0 to t produces the time-dependent position, $\mathbf{r}(t)$, written as

$$\mathbf{r}(t) = \int_0^t (\mathbf{v}_s(\tau) + \gamma^{-1} \xi(\tau)) d\tau, \quad (J2)$$

where we assume the initial position is zero. From Eq. (J2), the MSD is written as

$$\begin{aligned} \langle |\mathbf{r}(t)|^2 \rangle &= 2 \int_0^t d\tau (t - \tau) [\gamma^{-2} \langle \xi(\tau) \cdot \xi(0) \rangle + \langle \mathbf{v}_s(\tau) \cdot \mathbf{v}_s(0) \rangle] \\ &= 2d \int_0^t d\tau (t - \tau) [D_0 \tau_p^{-1} \phi_\xi(\tau) + D_a \tau_c^{-1} \phi_{\mathbf{v}_s}(\tau)] \\ &= \langle |\mathbf{r}_\xi(t)|^2 \rangle + \langle |\mathbf{r}_{\mathbf{v}_s}(t)|^2 \rangle, \end{aligned} \quad (J3)$$

where $\phi_\xi(t)$ denotes the normalized time-correlation function, $\langle \xi(t) \cdot \xi(0) \rangle / \langle \xi(0)^2 \rangle$, of the random fluctuating force, $\xi(t)$, and the relaxation time, τ_p , is defined as $\tau_p \equiv \int_0^\infty dt \phi_\xi(t)$. Here, the diffusion coefficient for passive motion is defined by $D_0 = d^{-1} \gamma^{-2} \int_0^\infty dt \langle \xi(t) \cdot \xi(0) \rangle$, and the diffusion coefficient for self-propelled motion is defined by $D_a = d^{-1} \int_0^\infty dt \langle \mathbf{v}_s(t) \cdot \mathbf{v}_s(0) \rangle$. The MSD consists of two independent movements from the random, thermal motion and the active, self-propelled motion. The diffusive mode contribution to the MSD is defined as $\langle |\mathbf{r}_\xi(t)|^2 \rangle \equiv 2d D_0 \tau_p^{-1} \int_0^t d\tau (t - \tau) \phi_\xi(\tau)$, while the self-propelled mode contribution is defined as $\langle |\mathbf{r}_{\mathbf{v}_s}(t)|^2 \rangle \equiv 2d D_a \tau_c^{-1} \int_0^t d\tau (t - \tau) \phi_{\mathbf{v}_s}(\tau)$. If we assume that the distribution of $\xi(t)$ is a Gaussian, then the analytic solution for the fourth moment of displacement can be written as

$$\langle |\mathbf{r}(t)|^4 \rangle = (1 + 2d^{-1}) \langle |\mathbf{r}_\xi(t)|^2 \rangle^2 + 2(1 + 2d^{-1}) \langle |\mathbf{r}_\xi(t)|^2 \rangle \langle |\mathbf{r}_{\mathbf{v}_s}(t)|^2 \rangle + \langle |\mathbf{r}_{\mathbf{v}_s}(t)|^4 \rangle, \quad (J4)$$

where $\langle |\mathbf{r}_{\mathbf{v}_s}(t)|^4 \rangle \equiv 4! \int_0^t dt_4 \int_0^{t_4} dt_3 \int_0^{t_3} dt_2 \int_0^{t_2} dt_1 \langle \mathbf{v}_s(t_4) \cdot \mathbf{v}_s(t_3) \mathbf{v}_s(t_2) \cdot \mathbf{v}_s(t_1) \rangle$. The NGP for the general model can be written as

$$\text{NGP}_R(t) \equiv \frac{d}{d+2} \frac{\langle |\mathbf{r}(t)|^4 \rangle}{\langle |\mathbf{r}(t)|^2 \rangle^2} - 1 = \frac{\langle |\mathbf{r}_{\mathbf{v}_s}(t)|^2 \rangle^2}{\langle |\mathbf{r}(t)|^2 \rangle^2} \text{NGP}_{\mathbf{v}_s}(t)$$

with

$$\text{NGP}_{\mathbf{v}_s}(t) \equiv \frac{d}{d+2} \frac{\langle |\mathbf{r}_{\mathbf{v}_s}(t)|^4 \rangle}{\langle |\mathbf{r}_{\mathbf{v}_s}(t)|^2 \rangle^2} - 1. \quad (J5)$$

At short times, $\text{NGP}_R(t)$ approaches zero because $\langle |\mathbf{r}(t)|^2 \rangle^2 \gg \langle |\mathbf{r}_{\mathbf{v}_s}(t)|^2 \rangle^2$. At long times, $\text{NGP}_R(t)$ also approaches zero because $\text{NGP}_{\mathbf{v}_s}(t)$ approaches zero.

APPENDIX K: STOCHASTIC SIMULATION METHOD

Our stochastic simulation method consists of both Brownian dynamics for the time evolution of an active matter position and the Gillespie method for the stochastic transition between internal states [60,61]. For Brownian dynamics, we numerically integrate Eq. (1) as

$$x(t + \Delta t) = x(t) + v(\Gamma) \Delta t + \sqrt{2D_0 \Delta t} \xi'(t), \quad (K1)$$

where $x(t)$, Δt , and $\xi'(t)$ denote the active matter position at time t , the size of the time step, and a Gaussian random number from the standard normal distribution, respectively [61]. For the Gillespie method, we assume that transitions between internal states for the multimode model are absent, except those transitions described by the following four unimolecular reactions:

$\Gamma_+ \xrightarrow{K_{+ \rightarrow 0} = k_{a0}} \Gamma_0, \Gamma_- \xrightarrow{K_{- \rightarrow 0} = k_{a0}} \Gamma_0, \Gamma_0 \xrightarrow{K_{0 \rightarrow +} = k_{0a}} \Gamma_+,$ and $\Gamma_0 \xrightarrow{K_{0 \rightarrow -} = k_{0a}} \Gamma_-$ [60]. The reaction constants for the absent transitions are set equal to zero. Our stochastic simulations proceed as follows:

(1) Randomly choose an internal state of active matter based on the equilibrium population between the states and set the initial position equal to zero. Set the selected state to the current state, Γ_c .

(2) Based on the current state, calculate the waiting time for a reaction using the equation, $\tau = -\ln(RN)/\sum_{j \neq c} K_{c \rightarrow j}$, where RN denotes an evenly distributed random number between 0 and 1, because concentration of the selected state is 1 and the concentration for the other states is zero. Only the Γ_0 state has two reaction paths with equal probability, and the other states have only one path for state transition.

(3) Evolve the time-dependent position using Eq. (K1) with the state-dependent velocity, $v(\Gamma_c)$, and a given time interval, Δt , until the waiting time, τ , has been reached.

(4) After finishing the time evolution, change the current state to the state determined by the transition in 2. Return to 2. when the elapsed time of the trajectory is less than the time limit of the trajectory.

(5) Repeat 1. until sufficient trajectories have been collected. We use 500 000 trajectories to obtain the velocity distributions and the second and fourth moments of the displacement distributions.

-
- [1] K. Chen, B. Wang, and S. Granick, *Nat. Mater.* **14**, 589 (2015).
- [2] K. Shin, S. Song, Y. H. Song, S. Hahn, J. H. Kim, G. Lee, I. C. Jeong, J. Sung, and K. T. Lee, *J. Phys. Chem. Lett.* **10**, 3071 (2019).
- [3] M. Theves, J. Taktikos, V. Zaburdaev, H. Stark, and C. Beta, *Biophys. J.* **105**, 1915 (2013).
- [4] D. Arcizet, B. Meier, E. Sackmann, J. O. Radler, and D. Heinrich, *Phys. Rev. Lett.* **101**, 248103 (2008).
- [5] M. S. Song, H. C. Moon, J. H. Jeon, and H. Y. Park, *Nat. Commun.* **9**, 344 (2018).
- [6] Y. Lanoiselee and D. S. Grebenkov, *J. Phys. A: Math. Theor.* **51**, 145602 (2018).
- [7] C. Loverdo, O. Benichou, M. Moreau, and R. Voituriez, *Nat. Phys.* **4**, 134 (2008).
- [8] P. Witzel, M. Gotz, Y. Lanoiselee, T. Franosch, D. S. Grebenkov, and D. Heinrich, *Biophys. J.* **117**, 203 (2019).
- [9] B. Wang, S. M. Anthony, S. C. Bae, and S. Granick, *Proc. Natl. Acad. Sci. USA* **106**, 15160 (2009).
- [10] O. Sliusarenko, J. Neu, D. R. Zusman, and G. Oster, *Proc. Natl. Acad. Sci. USA* **103**, 1534 (2006).
- [11] Y. Wu, A. D. Kaiser, Y. Jiang, and M. S. Alber, *Proc. Natl. Acad. Sci. USA* **106**, 1222 (2009).
- [12] J. E. Johansen, J. Pinhassi, N. Blackburn, U. L. Zweifel, and A. Hagstrom, *Aquat. Microb. Ecol.* **28**, 229 (2002).
- [13] R. Grossmann, F. Peruani, and M. Bar, *New J. Phys.* **18**, 043009 (2016).
- [14] A. Yildiz, J. N. Forkey, S. A. McKinney, T. Ha, Y. E. Goldman, and P. R. Selvin, *Science* **300**, 2061 (2003).
- [15] S. H. Nam, Y. M. Bae, Y. I. Park, J. H. Kim, H. M. Kim, J. S. Choi, K. T. Lee, T. Hyeon, and Y. D. Suh, *Angew. Chem. Int. Ed. Engl.* **50**, 6093 (2011).
- [16] H. L. Jo, Y. H. Song, J. Park, E. J. Jo, Y. Goh, K. Shin, M. G. Kim, and K. T. Lee, *Nanoscale* **7**, 19397 (2015).
- [17] A. Einstein, *Ann. Phys.* **322**, 549 (1905).
- [18] N. Wax, *Selected Papers on Noise and Stochastic Processes* (Dover Publications, New York, 1954).
- [19] M. H. Gail and C. W. Boone, *Biophys. J.* **10**, 980 (1970).
- [20] C. L. Stokes, D. A. Lauffenburger, and S. K. Williams, *J. Cell Sci.* **99**, 419 (1991).
- [21] L. Li, S. F. Norrelykke, and E. C. Cox, *PLoS ONE* **3**, e2093 (2008).
- [22] X. Liu, E. S. Welf, and J. M. Haugh, *J. R. Soc. Interface* **12**, 20141412 (2015).
- [23] R. Metzler and J. Klafter, *Phys. Rep.* **339**, 1 (2000).
- [24] F. Thiel, L. Schimansky-Geier, and I. M. Sokolov, *Phys. Rev. E* **86**, 021117 (2012).
- [25] I. G. Portillo, D. Campos, and V. Méndez, *J. Stat. Mech.* (2011) P02033.
- [26] G. Zumofen and J. Klafter, *Phys. Rev. E* **51**, 1818 (1995).
- [27] R. Metzler, J. H. Jeon, A. G. Cherstvy, and E. Barkai, *Phys. Chem. Chem. Phys.* **16**, 24128 (2014).
- [28] L. Schimanskygeier, M. Mieth, H. Rose, and H. Malchow, *Phys. Lett. A* **207**, 140 (1995).
- [29] P. Romanczuk, M. Bar, W. Ebeling, B. Lindner, and L. Schimansky-Geier, *Eur. Phys. J. Spec. Top.* **202**, 1 (2012).
- [30] S. Goldstein, *Q. J. Mech. Appl. Math.* **4**, 129 (1951).
- [31] H. Takagi, M. J. Sato, T. Yanagida, and M. Ueda, *PLoS ONE* **3**, e2648 (2008).
- [32] J. R. Howse, R. A. L. Jones, A. J. Ryan, T. Gough, R. Vafabakhsh, and R. Golestanian, *Phys. Rev. Lett.* **99**, 048102 (2007).
- [33] D. Selmeczi, L. Li, L. I. I. Pedersen, S. F. Nrrelykke, P. H. Hagedorn, S. Mosler, N. B. Larsen, E. C. Cox, and H. Flyvbjerg, *Eur. Phys. J. Spec. Top.* **157**, 1 (2008).
- [34] D. Campos, V. Mendez, and I. Llopis, *J. Theor. Biol.* **267**, 526 (2010).
- [35] O. Benichou, M. Coppey, M. Moreau, P. H. Suet, and R. Voituriez, *Phys. Rev. Lett.* **94**, 198101 (2005).
- [36] J. M. Newby and P. C. Bressloff, *Phys. Rev. E* **80**, 021913 (2009).
- [37] O. Benichou, C. Loverdo, M. Moreau, and R. Voituriez, *Rev. Mod. Phys.* **83**, 81 (2011).
- [38] P. C. Bressloff and J. M. Newby, *Rev. Mod. Phys.* **85**, 135 (2013).
- [39] M. A. Lomholt, T. Koren, R. Metzler, and J. Klafter, *Proc. Natl. Acad. Sci. USA* **105**, 11055 (2008).
- [40] A. Weron, K. Burnecki, E. J. Akin, L. Sole, M. Balcerek, M. M. Tamkun, and D. Krapf, *Sci. Rep.* **7**, 5404 (2017).
- [41] T. Sungkaworn, M. L. Jobin, K. Burnecki, A. Weron, M. J. Lohse, and D. Calebiro, *Nature (London)* **550**, 543 (2017).
- [42] P. C. Bressloff, *J. Phys. A: Math. Theor.* **50**, 133001 (2017).

- [43] Y. Lanoiselee and D. S. Grebenkov, *J. Phys. A: Math. Theor.* **52**, 304001 (2019).
- [44] D. S. Grebenkov, *Phys. Rev. E* **99**, 032133 (2019).
- [45] H. Risken, *The Fokker-Planck Equation: Methods of Solution and Applications*, 2nd ed., Springer Series in Synergetics Vol. 18 (Springer-Verlag, New York, 1996).
- [46] S. I. Denisov, W. Horsthemke, and P. Hanggi, *Eur. Phys. J. B* **68**, 567 (2009).
- [47] J. Kang, S. Song, and S. Hahn, *J. Korean Phys. Soc.* **73**, 242 (2018).
- [48] Y. R. Lim, J. H. Kim, S. J. Park, G. S. Yang, S. Song, S. K. Chang, N. K. Lee, and J. Sung, *Phys. Rev. X* **5**, 031014 (2015).
- [49] D. A. McQuarrie, in *Statistical Mechanics* (University Science Books, Sausalito, CA, 2000), pp. 380–381.
- [50] M. J. Schnitzer, *Phys. Rev. E* **48**, 2553 (1993).
- [51] J. Tailleur and M. E. Cates, *Phys. Rev. Lett.* **100**, 218103 (2008).
- [52] S. Mukamel, *Principles of Nonlinear Optical Spectroscopy*, Oxford Series in Optical and Imaging Sciences Vol. 6 (Oxford University Press, New York, 1995).
- [53] F. J. Sevilla and L. A. Gomez Nava, *Phys. Rev. E* **90**, 022130 (2014).
- [54] X. Zheng, B. ten Hagen, A. Kaiser, M. Wu, H. Cui, Z. Silber-Li, and H. Lowen, *Phys. Rev. E* **88**, 032304 (2013).
- [55] H. G. Othmer, S. R. Dunbar, and W. Alt, *J. Math. Biol.* **26**, 263 (1988).
- [56] F. J. Sevilla and M. Sandoval, *Phys. Rev. E* **91**, 052150 (2015).
- [57] B. ten Hagen, S. van Teeffelen, and H. Lowen, *J. Phys.: Condens. Matter* **23**, 194119 (2011).
- [58] B. Wang, J. Kuo, S. C. Bae, and S. Granick, *Nat. Mater.* **11**, 481 (2012).
- [59] R. Metzler, *Phys. Rev. E* **62**, 6233 (2000).
- [60] D. T. Gillespie, *J. Phys. Chem.* **81**, 2340 (1977).
- [61] D. L. Ermak, *J. Chem. Phys.* **62**, 4189 (1975).